HHS Public Access

Author manuscript

*Acta Biomater*. Author manuscript; available in PMC 2020 November 01.

Published in final edited form as:

*Acta Biomater*. 2019 November ; 99: 100–109. doi:10.1016/j.actbio.2019.09.018.

# Incorporation of a silicon-based polymer to PEG-DA templated hydrogel scaffolds for bioactivity and osteoinductivity

**Michael T. Frassica**[a], **Sarah K. Jones**[a], **Patricia Diaz-Rodriguez**[b], **Mariah S. Hahn**[b], **Melissa A. Grunlan**[a,c,d,e,*]

[a]Department of Biomedical Engineering, Texas A&M University, College Station, TX 77843-3120 (USA)

[b]Department of Biomedical Engineering, Rensselaer Polytechnic Institute, Troy, NY 12180-31590 (USA)

[c]Department of Materials Science & Engineering, Texas A&M University, College Station, TX 77843-3003 (USA)

[d]Center for Remote Health Technologies Systems, Texas A&M University, College Station, TX 77843-3577 (USA)

[e]Department of Chemistry, Texas A&M University, College Station, TX 77843-3255 (USA)

## Abstract

A scaffold that is inherently bioactive, osteoinductive and osteoconductive may guide mesenchymal stem cells (MSCs) to regenerate bone tissue in the absence of exogenous growth factors. Previously, we established that hydrogel scaffolds formed by crosslinking methacrylated star poly(dimethylsiloxane) ($PDMS_{star}$-MA) with poly(ethylene glycol) (PEG-DA) promote bone bonding by induction of hydroxyapatite formation ("bioactive") and promote MSC lineage progression toward osteoblast-like fate ("osteoinductive"). Herein, we have combined solvent induced phase separation (SIPS) with a fused salt template to create $PDMS_{star}$-PEG hydrogel scaffolds with controlled $PDMS_{star}$-MA distribution as well as interconnected macropores of a tunable size to allow for subsequent cell seeding and neotissue infiltration ("osteoconductive"). Scaffolds were prepared with $PDMS_{star}$-MA of two number average molecular weights ($M_n$s) (2k and 7k) with varying $PDMS_{star}$-MA:PEG-DA ratios and template salt sizes. The distribution of $PDMS_{star}$-MA within the hydrogels was examined as well as pore size, percent interconnectivity, dynamic and static moduli, hydration, degradation and *in vitro* bioactivity (i.e. mineralization when exposed to simulated body fluid, SBF). Finally, cell culture with seeded human bone marrow-derived MSCs (hBMSCs) was used to confirm non-cytotoxicity and characterize osteoinductivity. Tunable, interconnected macropores were achieved by utilization of a fused salt template of a specified salt size during fabrication. Distribution of $PDMS_{star}$-MA within the PEG-DA matrix improved for the lower $M_n$ and contributed to differences in specific material properties

*Corresponding author: Prof. M. A. Grunlan, Tel: 01 979 845 2406, Fax: 01 979 845 4450, mgrunlan@tamu.edu.

(e.g. local modulus) and cellular response. However, all templated SIPS $PDMS_{star}$-PEG hydrogels were confirmed to be bioactive, non-cytotoxic and displayed $PDMS_{star}$-MA dose-dependent osteogenesis.

## Graphical Abstract

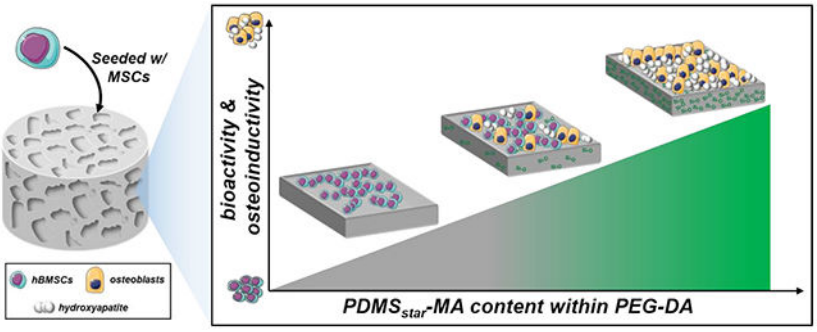


A tissue engineering scaffold that can inherently guide mesenchymal stem cells (MSCs) to regenerate bone tissue without growth factors would be a more cost-effective and safe strategy for bone repair. Typically, glass/ceramic fillers are utilized to achieve this through their ability to induce hydroxyapatite formation (“bioactive”) and promote MSC differentiation to an osteoblast-like fate (“osteoinductive”). Herein, we have fabricated an interconnected, macroporous PEG-DA hydrogel scaffold that utilizes $PDMS_{star}$-MA as a bioactive and osteoinductive scaffold component. We were able to show that these $PDMS_{star}$-PEG hydrogels maintain several key material characteristics for bone repair. Further, bioactivity and osteoinductivity were simultaneously achieved in human bone marrow-derived MSC culture, representing a notable achievement for an exclusively material-based strategy.

### Keywords

Poly(ethylene glycol); Poly(dimethylsiloxane); Salt templating; Scaffold; Tissue engineering

## 1. Introduction

Bone tissue regeneration holds potential to be achieved with an instructive scaffold whose chemical and physical properties direct the behavior of associated mesenchymal stem cells (MSCs), even in the absence of exogenous growth factors [1–3]. This “materials-based” approach to bone regeneration would mitigate cost and risks of off-target responses associated with added growth factors [4–6]. Ideally, such a scaffold would be osteoinductive (to stimulate differentiation of cells into the bone-forming lineage), bioactive (to promote bonding with adjacent bone tissue by hydroxyapatite mineralization) and osteoconductive (to permit bone growth on its surface or down into pores) [7–9]. Osteoconductivity may be obtained when scaffolds are produced with optimized pore size (i.e. between 200 and 400 μm) as well as pore interconnectivity [10–12]. Approaches to achieve osteoinductivity and bioactivity have often relied on the incorporation of inorganic and hydrophobic materials, particularly bioactive glasses and ceramics used as fillers [13–16]. However, such composite scaffolds typically suffer from low fracture toughness, limited or low resorption rates and a

lack of ideal pore features [7, 17]. Scaffolds that mitigate these issues while achieving these instructive behaviors would represent a significant advancement in bone regeneration.

It has been demonstrated that silicon plays a key role in bone mineralization and gene activation [18, 19], thus prompting the use of certain glasses or ceramics. Instead, we have demonstrated that bioactivity and osteoinductivity could be obtained by introducing silicon-based, inorganic polymer to a conventional organic hydrogel [20, 21]. Specifically, inorganic star poly(dimethylsiloxane) methacrylate ($PDMS_{star}$-MA) was introduced to organic poly(ethylene glycol) diacrylate (PEG-DA) to form $PDMS_{star}$-PEG hydrogels [20, 22], up to a 30:70 wt/wt % ratio of $PDMS_{star}$-MA:PEG-DA. As “biological blank slates”, resisting non-specific protein and cell adhesion, PEG-DA hydrogels have been extensively studied as instructive scaffolds [23, 24]. To control cell adhesion, cell adhesive ligands, such as the peptide RGDS, can be readily introduced [25]. In this way, specific material properties (e.g. stiffness and hydration) may be tuned and readily correlated to associated cellular responses. However, PEG-DA hydrogels lack inherent osteoinductivity and bioactivity. On the other hand, the $PDMS_{star}$-PEG hydrogels maintained the biological blank slate nature of PEG-DA hydrogels but also induced osteogenic responses of photoencapsulated bone marrow-derived mesenchymal stem cells (BMSCs) [20–22]. Due to the insolubility of $PDMS_{star}$-MA in the aqueous precursor solution, it was heterogeneously distributed as microdroplets throughout the PEG-DA matrix [22]. Thus, to improve $PDMS_{star}$-MA distribution, these hydrogels were later prepared via solvent induced phase separation (SIPS) by employing an organic solvent (dichloromethane, DCM) to prepare the precursor solutions [20, 26]. Following sequential UV-cure, removal of the DCM and hydration, the resulting SIPS $PDMS_{star}$-PEG hydrogels revealed improved $PDMS_{star}$ distribution as well as the presence of pores of increased size (up to ~200 μm) with $PDMS_{star}$-MA content. However, these pores lacked interconnectivity necessary for cell seeding and eventual neotissue infiltration [20].

Herein, we sought to produce instructive $PDMS_{star}$-PEG hydrogels - having controlled porosity and pore interconnectivity as well as enhanced distribution of $PDMS_{star}$-MA - by fabrication via SIPS in combination with a fused salt template. Tight control over pore size and maximized pore interconnectivity has been shown to be achieved with fused salt templates [27, 28]. Our recent work has shown that templating is effective to prepare SIPS PEG-DA hydrogels with interconnected macropores of tunable sizes >100 μm [29]; however, these hydrogels remain lacking in osteoinductivity and bioactivity. Thus, we prepared a series of templated SIPS $PDMS_{star}$-PEG-DA hydrogels based on different number average molecular weights ($M_n$) of $PDMS_{star}$-MA (2k and 7k). These were incorporated into a DCM-based precursor solution at increasing wt/wt % ratios (0:100, 10:90, 20:80, and 30:70) of $PDMS_{star}$-MA to PEG-DA ($M_n$ = 3.4k). The distribution of $PDMS_{star}$-MA was evaluated along with the ability to achieve tunable pore size and pore interconnectivity. The effect of templated SIPS hydrogel composition on hydration and modulus was examined, as these material properties are known to influence cellular behavior [30–33]. The bioactivity and degradation rates were also investigated. Scaffolds were further evaluated to confirm non-cytotoxicity and degree of osteogenic capacity after seeding with human bone marrow derived mesenchymal stem cells (hBMSCs).

## 2. Materials and Methods

### 2.1. Materials

1-Vinyl-2-pyrrolidinone (NVP), 2,2-dimethyl-2-phenylacetophenone (DMAP), acryloyl chloride, allyl methacrylate, calcium chloride, dibasic potassium phosphate, HC1 (12 M), hexamethyldisilazane (HMDS), magnesium chloride hexahydrate, magnesium sulfate, NaOH, Nile red, NMR grade, deuterated chloroform ($CDCl_3$), poly(ethylene glycol) 3350 (PEG-3350), potassium carbonate, potassium chloride, silica gel, sodium bicarbonate, sodium chloride (salt), sodium sulfate, triethylamine, trifluoromethanesulfonic acid (triflic acid), tris-hydroxymethyl aminomethane, Triton X-100 (0.1%) and all solvents were obtained from Sigma-Aldrich. HPLC-grade toluene, dichloromethane, and NMR grade $CDCl_3$ were dried over 4 Å molecular sieves. Salt was sieved (ASTM E-11 Specification, No. 40, 425 μm opening; No. 60 250 μm opening) to obtain the following salt sizes: “small salt” (SS): 181 ± 29 μm, “medium salt” (MS): 268 ± 35 μm and “large salt” (LS): 459 ± 69 μm. Average salt sizes were calculated using ImageJ software, as done previously [29]. Silver nitrate and sodium thiosulfate were obtained from American Mastertech. Fetal bovine serum (16.5%; FBS) was obtained from Atlanta Biologicals. Glutamax, Minimum Essential Medium Alpha (α-MEM), Penicillin-Streptomycin and 1% glutamine (Glutamex) were obtained from Gibco. Phosphate-buffered saline (1X without Ca and Mg; PBS) and Dulbecco’s Modified Eagle Media (DMEM) was obtained from Corning. Octamethylcyclotetrasiloxane ($D_4$), Pt-divinyltetramethyldisiloxane complex in 2 wt% xylene (Karstedt’s catalyst), and tetrakis(dimethylsiloxy)silane (tetra-SiH) were obtained from Gelest. Activated carbon, buffered formalin, DAPI, dialysis cassettes (3.5k MWCO), anhydrous ethyl ether, and rhodamine phalloidin were obtained from Fisher Scientific. Von Kossa staining kit was obtained from American Mastertech Scientific. Acryloyl-PEG-succinimidyl valerate was obtained from Laysan Bio, Inc. Dulbecco’s phosphate-buffered saline (DPBS) was obtained from Lonza. Peptide RGDS was obtained from Bachem. Cytotoxicity detection kit (LDH) was obtained from Roche, multiplex immunoassay kits were obtained from R&D Systems and the PicoGreen assay kit was obtained from Invitrogen.

### 2.2. Synthesis

**2.2.1. $PDMS_{star}$-MA synthesis—**$PDMS_{star}$-MA ($M_n$ = 2k and 7k g/mol) were prepared as previously reported [20, 22]. First, Silane (SiH)-terminated $PDMS_{star}$ was prepared by the acid-catalyzed equilibration of $D_4$ (“2k”: 30.0 g, 101.4 mmol; “7k”: 29.9 g, 101.0 mmol) with tetra-SiH (“2k”: 7.8 g, 23.8 mmol; “7k”: 1.1 g, 3.4 mmol) utilizing triflic acid (60 μl) and subsequent neutralization with HMDS (0.15 g, 0.93 mmol). The resulting $PDMS_{star}$-SiH (for “2k” and “7k”) were each precipitated three times in toluene/methanol and dried under reduced pressure, resulting in a colorless liquid. Next, photoreactive groups were added via hydrosilylation to the terminal ends of each arm of $PDMS_{star}$-SiH (“2k”: 7.0 g, 2.5 mmol; “7k”: 7.0 g, 0.53 mmol) by Pt-catalyzed [Karstedt’s catalyst (50 μL)] reaction with allyl methacrylate (“2k”: 3.6 mL, 26.8 mmol; “7k”: 0.314 mL, 2.33 mmol) in toluene (30 mL). Both $M_n$’s of $PDMS_{star}$-MA were obtained after a 2 hour activated carbon spin and flash column chromatography. The structures of each $M_n$ of $PDMS_{star}$-SiH and $PDMS_{star}$-MA were confirmed by $^1H$ NMR and was in agreement with that previously reported.

**2.2.2. PEG-DA synthesis—**PEG-DA ($M_n$ = 3.4k g/mol) was prepared as previously reported [22]. PEG-3350 (23.5 g, 7.0 mmol) was dissolved in DCM, then triethylamine (1.95 mL, 14.0 mmol) and subsequently acryloyl chloride (2.27 mL, 28.0 mmol) were added dropwise to the solution and allowed to react overnight. HCl was removed by 2M $k_2CO_3$ wash in a separatory funnel. The reaction was then dried in the organic phase with $MgSO_4$ spin and precipitated in anhydrous ethyl ether. After vacuum filtration to obtain the white solid, PEG-DA was vacuum dried to remove residual solvent. The structure was confirmed by $^1$H NMR and was in agreement with that previously reported.

**2.2.3. ACRL-PEG-RGDS synthesis—**ACRL-PEG-RGDS was synthesized as previously reported [21]. The cell adhesion peptide RGDS was reacted with acryloyl-PEG-SVA at a 1:1 molar ratio for 2 hr in 50 mM sodium bicarbonate buffer. ACRL-PEG-RGDS was purified by dialysis, lyophilized, and stored at −20°C under nitrogen ($N_2$). ACRL-PEG-RGDS was included in all hydrogels utilized for cell culture at 1 μmol/mL of precursor solution.

## 2.3. NMR

$^1$H-NMR spectra were obtained on an INOVA 500 500 MHz spectrometer operating in the Fourier transform mode. Solutions of 5% (w/v) $CDCl_3$ were used to obtain spectra. Residual $CHCl_3$ served as an internal standard.

## 2.4. Salt template formation

Salt templates were formed with each of the three average salt sizes: “small salt” (~180 μm), “medium salt” (~270 μm) and “large salt” (~460 μm). Molds for making the salt template and subsequently curing the precursor solution were prepared as follows. One end of a borosilicate glass tube (5/8” OD, 1/2” ID, 1.5” H) was covered with aluminum foil, pushed into a custom Teflon cap (1” OD, 5/8” ID) that contained a small hole (0.05” D) directly through its center and then tightly wrapped with Parafilm to secure the glass tube to the cap (Fig. S1). Salt of the designated size (16 g) was mixed gently with 5 wt% DI water (using a metal spatula) in a 25 mL beaker and 3.5 g of the mixture added to the mold. The salt mixture was then compacted into the mold using a flat-ended glass rod, covered with Parafilm, and centrifuged 5 min at 2000 rpm within a 50 mL centrifuge tube (Eppendorf 5810R centrifuge, A-4-62 rotor). Afterwards, the Parafilm cover was removed and the fused template allowed to air dry at room temperature (RT) for 24 hr within the glass mold.

## 2.5. Templated hydrogel fabrication

DCM-based precursor solutions were prepared containing 30 wt% total macromer (based on total solution mass) with increasing wt/wt % ratios of $PDMS_{star}$-MA to PEG-DA: 0:100 (PEG-DA control), 10:90, 20:80, and 30:70. Photoinitiator solution (30 wt% DMAP in NVP) was added at 100 μL/g of macromer. Solutions were vortexed in a sealed vial for 1 min after addition of each component. The precursor solution (~1.5 mL) was immediately deposited atop the aforementioned dried salt template via syringe. After ~30 s, the aluminum foil at the base of the mold was punctured through the hole in the Teflon cap. Using PVC tubing (3/8” ID, 9/16” OD) held against the top of the glass mold, compressed air was used to gently force the solution throughout the salt template until the solution began to exit

through the cap hole. Removal of the air inlet caused the flow of precursor solution to cease. The filled mold was UV-cured for 15 min (12 min standing on Teflon cap and 3 min standing on the glass top) via exposure to a UV-transilluminator (6 mW $cm^2$, 365 nm). After air-drying 24 hr to evaporate the solvent, the cylindrical specimen was removed from the mold and sectioned into 1.2 mm thick discs using a vibratome (Leica VT1000S; cutting speed = 1.75 mm/s; frequency = 30 Hz). Only discs from the central portion of the cylinder were used for testing, discarding ~4 mm from each end. Discs were soaked in DI water for 48 hr on a rocker table (100 rpm; water changes 3X daily) to leach the salt template and swell the hydrogels to their final hydrated form (~15 mm diameter, ~1.5 mm thick). Discs were allowed to soak an additional 72 hr prior to testing, for which they were punched to a desired size (8 or 13 mm) from the central region of the disc using a die.

### 2.6. Sol content

Discs (N = 5; 13 mm diameter) were air dried 30 min. Each disc was placed in an open scintillation vial and dried at RT in a vacuum oven (14.7 psi, 24 hr). Dried discs were weighed ($W_{d1}$), placed in a new scintillation vial with 10 mL of DCM, and set on a rocker table (100 rpm) for 48 hr. Removed discs were placed in new scintillation vials, allowed to air dry (30 min) and dried again at RT in the vacuum oven (14.7 psi, 24 h). The final weight was taken ($W_{d2}$) and the sol content calculated as $[(W_{d1} - W_{d2})/W_{d1}] \times 100$.

### 2.7. Equilibrium swelling

Discs (N = 5; 13 mm diameter) were each placed in a sealed vial with 15 mL of DI water on a rocker table (100 rpm) for 48 hr at RT. Discs were then removed and weighed ($W_s$). Discs were dried (14.7 psi, 60 °C, 24 hr) and weighed again ($W_d$). Equilibrium swelling ratio was calculated as $(W_s - W_d)/W_d$.

### 2.8. Distribution of $PDMS_{star}$-MA and pore morphology

**2.8.1. Confocal laser scanning microscopy (CLSM)—**Discs (8 mm diameter) were soaked for 24 hr in 60 mL Nile Red solution, followed by daily changes with PBS for 3 days. Nile red solution contains 75 μL of a solution containing 20 mg Nile Red and 1 mL methanol mixed into 8 mL of DI water and added to 120 mL of PBS, as previously reported [20]. Discs were placed in a coverglass-bottom chamber and imaged on an Olympus FV1000 confocal microscope, equipped with a UPLSAPO 10x/0.4 objective. Excitation and emission were 488 nm and 500-600 nm, respectively. The confocal aperture was set to 1 Airy unit. Z-stacks (80 slices) were acquired with a 4.0 μm step. Confocal zoom and resolution setting resulted in XY pixel size of 2.485 μm. Representative slices of the stacks were exported. The fluorescence images were pseudo-colored green. Bright field imaging was conducted simultaneously and used to measure hydrated pore size. Images were taken of three locations on two different samples for each salt size (20:80 wt/wt% $PDMS_{star}$-MA:PEG-DA) with one pore measured per image (N = 6). ImageJ Software was used to calculate pore size, determined by the mean of the diagonal and central cross-section.

**2.8.2. Scanning electron microscopy (SEM)—**Discs (8 mm diameter) were allowed to air dry (30 min), and dried in a vacuum oven (14.7 psi, 24 hr, RT). Dried discs were subjected to Au-sputter coating (Cressington Sputter Coater 108) and viewed with a field

emission scanning electron microscope (FE-SEM; JEOL NeoScope JCM-5000) at an accelerated electron energy of 10 keV. Pore size was measured using ImageJ software, and determined by the mean of the longest and shortest cross-sectional areas of the rectangular pores. Dry pore measurement was conducted by the same method described in section 2.8.1.

**2.8.3. Percent interconnectivity—**Discs (N = 3; 13 mm diameter) were evaluated to determine interconnectivity with a water wicking procedure adapted from *Bencherif et al.* [34]. Each disc was soaked for 24 hr in DI water on a rocker table (100 rpm) to ensure no air bubbles existed within pores. Discs were removed and weighed in a glass Petri dish ($W_{total}$). A folded Kimwipe was then gently pressed on the disc for 1 min to wick away the interconnected volume, and the disc was weighed again ($W_{interconnected}$). Percent interconnectivity was calculated as $[(W_{total} - W_{interconnected})/W_{total}] \times 100$.

## 2.9. Mechanical properties

**2.9.1. Bulk compressive Young's modulus and damping – static and dynamic mechanical analysis—**Discs (8 mm diameter) were used for the measurement of Young's modulus (N = 4) as well as dynamic moduli (N = 8) using a dynamic mechanical analyzer (DMA; TA Instruments Q800) with a parallel-plate compression clamp equipped with plates of 40 mm (bottom) and 15 mm (top). Hydrated discs were placed between the plates and several drops of DI water were dropped onto the hydrogel to maintain hydration. Analyses were conducted at RT. For static testing, samples were tested at RT in a controlled strain rate mode (20%/min to 12% strain) with a preload force of 0.1 N. Young's modulus was obtained from the slope of the linear portion of the stress-strain curve (1-5%). For dynamic testing, samples were tested using a multi-frequency strain mode (1-30 Hz) with an amplitude of 10 μm and preload force of 0.1 N. The obtained values of loss (G") and storage (G') were used to calculate tan δ (i.e. damping).

**2.9.2. Local Young's modulus - Atomic force microscopy (AFM)—**Discs (N = 2; 8 mm diameter) were used to measure local Young's modulus using a Dimension ICON AFM (Bruker) with a Nanoscope V controller. A modified silicon nitride probe (NovaScan, USA) having a nominal spring constant of 0.6 N/m with a 5 μm diameter bead attached to the cantilever was used. Standard detector calibration was performed on a clean mica disc to determine deflection sensitivity. Standard thermal tuning calculated a spring constant of ~0.75-0.9 N/m. For each sample, hydrogels were fixed to 15 mm metal AFM specimen discs (Ted Pella, Inc.) with water droplets added to the sample surface to maintain hydration. Indentation was carried out at the pore walls using 1 Hz loading rates. The ramp size was 1 μm and the indentation force was 15 nN. Young's modulus values were calculated using Nanoscope Analysis software (Bruker) with a Hertzian fit model after baseline correction and boxcar filter. A sample Poisson's ratio of 0.5 was used. Individual force-displacement curves were taken 6 times at each sampled point of the hydrogel, with 5 total points from 2 hydrogels sampled.

## 2.10. Accelerated degradation

Discs (N = 3 per time point; 8 mm diameter) underwent accelerated degradation analysis All hydrogel discs were vacuum dried (14.7 psi, 12 hr) and weighed. Each disc was then placed

in a 1 dram vial with 1 mL of 0.05M NaOH and stored in a shaking incubator (100 rpm, 37 °C). At 12 hr time points, one disc was removed, dried (14.7 psi, 12 hr), and weighed to determine mass loss percentage. At each time point, solutions for all samples were exchanged with new 0.05M NaOH.

## 2.11. Bioactivity

**2.11.1. Simulated body fluid (SBF) soak—**SBF was fabricated as detailed by *Kokubo et al.* and in previous studies [20, 35]. Individual discs (N = 2; 8 mm diameter) were placed in sealed 50 mL centrifuge tubes containing 40 mL of 1X SBF and incubated in a water bath at 37 °C. Discs were removed after 4 weeks, washed with DI water and vacuum dried (14.7 psi, 24 hr). Dried hydrogels were subjected to SEM imaging (section 2.8.2) and X-ray diffraction spectroscopy (section 2.11.2).

**2.11.2. X-ray diffraction spectroscopy (XRD)—**Powder X-ray diffraction data was collected on a Bruker D8 diffractometer fitted with a LynxEYE detector. The X-ray source was a 1kW Cu X-ray tube maintained at an operating current of 40 kV and 25 mA (Bragg-Brentano geometry; scan range 3 – 70 °; step size: 0.015 °).

## 2.12. Cell culture

Bone marrow derived human mesenchymal stem cells (hBMSCs) were obtained from the Texas A&M Institute for Regenerative Medicine. By flow cytometry, hBMSCs tested positive (> 95%) for CD29, CD44, CD49c, CD59, CD73a, CD90, CD105, CD146, CD147, CD166, and HLA-I:ABC and negative (< 5%) for CD3, CD11b, CD14, CD19, CD34, CD36, CD45, CD49b, CD49d, CD79a, CD106, CD184, CD271, HLA-II:DR, and HGFR (c-Met). hBMSCs were expanded in α-MEM supplemented with 16.5% FBS and 1% glutamine. Twenty-four hr prior to seeding, cells at passage 4 were transitioned to DMEM containing 10% FBS and 1% Penicillin/Streptomycin (P/S)).

## 2.13. Seeding and culture of scaffold constructs

Scaffolds were fabricated with ACRL-PEG-RGDS (section 2.2.3), and cut to 8 mm discs. Scaffolds were seeded with hBMSCs at 5xl$0^6$ cells/mL and cultured at 37 °C and 5% $CO_2$ in DMEM containing 10% FBS and 1% P/S. Culture medium was exchanged every 2 days through the duration of culture. Osteogenic supplements were not utilized so as to assess the intrinsic osteogenic potential of the scaffolds.

## 2.14. Cytotoxicity

Cytotoxicity assessments were performed after 48 hr culture by measuring the secretion of lactate dehydrogenase (LDH) with a commercial kit. Briefly, cell culture supernatants were collected, reacted with the kit working solution, and absorbance was measured following 25 min of development. Cell morphology and distribution were also evaluated after 48 hr of culture. Scaffolds were washed with DPBS and fixed with 10% buffered formalin. Fixed cells were then washed twice with DPBS and permeabilized with 0.1% Triton X-100. Cell distribution was evaluated after SYBR Green staining while cell morphology was assessed

by rhodamine phalloidin and DAPI staining. Confocal images were taken to evaluate both stains using a multiphoton microscope (Zeiss LSM 510Meta).

### 2.15. Endpoint construct analyses

Samples were collected after 48 hr (cytotoxicity) or 14 days of culture (osteogenic potential) by rinsing them with DPBS and snap freezing with liquid $N_2$. Scaffolds were stored at −80 °C until analysis. Protein samples were extracted by sample homogenization in lysis buffer and collection of the correspondent supernatant after centrifugation.

**2.15.1 Biochemical analyses—**hBMSC protein expression was evaluated by means of specific multiplex immunoassay kits following manufacturer's instructions. Proteins selected for analysis included Collagen 1A1 and osteonectin (secreted protein acidic and rich in cysteine; SPARC) for both 2k and 7k $PDMS_{star}$-MA containing scaffolds, and additionally osteopontin (OPN) and bone morphogenic protein-2 (BMP-2) for exclusively 2k $PDMS_{star}$-MA containing scaffolds. Samples were properly diluted with the assay buffer and loaded into well plates containing the appropriate bead suspension. Bound analyte was then reacted with detection antibodies, followed by the addition of streptavidin-phycoerythrin. Protein concentrations were determined by the median fluorescence intensity (MFI) using a MAGPIX (Luminex) in comparison to an analyte-specific standard curve. The obtained values were normalized to the DNA content of each construct and assessed via PicoGreen assay.

**2.15.2. Histological analyses—**Von Kossa staining was used to assess cellular calcium deposition by manufacturer's protocol. Rehydrated sections were rinsed with distilled water, after which a 5% silver nitrate solution was applied, followed by the exposure of the samples to full-spectrum light for 1 hr. Samples were then sequentially rinsed with distilled water, exposed to 5% sodium thiosulfate for 3 min, and rinsed with distilled water.

### 2.16. Statistics

Data is reported as the mean ± standard deviation. Data set mean values were compared in GraphPad Prism via ANOVA followed by Tukey's post hoc test where $p$-value < 0.05 was considered statistically significant.

## 3. Results and Discussion

### 3.1. SIPS/salt fabrication

Templated SIPS $PDMS_{star}$-PEG hydrogels were prepared by photocuring a DCM-based precursor solution over a fused salt template followed by sequential evaporation of the DCM solvent, template dissolution and hydration. Series of hydrogels were prepared based on different salt sizes ("small" ~180, "medium" ~270 and "large" ~460 μm) as well as two different $M_n$'s of $PDMS_{star}$-MA (2k and 7k) wherein the wt/wt % ratio of $PDMS_{star}$-MA to PEG:DA was systematically increased: 0:100, 10:90, 20:80 and 30:70. In our previous report, templated SIPS PEG-DA scaffolds (i.e. no $PDMS_{star}$-MA) were similarly prepared using a combination of SIPS and a fused salt template based on these salt sizes [29]. It was determined that a macromer concentration of 30% (wt/wt) in DCM produced mechanically

robust, macroporous hydrogels. This is in contrast to fabrication of conventional hydrogels from aqueous precursor solutions without a salt template, where macromer concentrations of ~5-15% (wt/wt) produce robust hydrogels owing to their low porosity [22, 36]. When we previously prepared non-templated SIPS $PDMS_{star}$-PEG hydrogels, the total macromer concentration was only 10% (wt/wt) in DCM [20]. However, in the present study, when the total macromer concentration was increased to 30% (wt/wt), this resulted in extremely hazy precursor solutions, particularly as the concentration and $M_n$ of $PDMS_{star}$-MA increased. Moreover, within several minutes, the solution exhibited signs of substantial phase separation, partitioning into a clear (i.e. $PDMS_{star}$-MA-rich layer) and cloudy layer (Fig. S2). Thus, it was critical to increase the flow rate of the precursor solution through the fused salt template so that it could be promptly photocured. Previously, the salt template was prepared in a glass vial and the precursor solution distributed through the template by centrifuging for 10 min [29]. Instead, herein, a mold was prepared from a glass tube and a Teflon cap (containing a small hole) secured to the base. After addition of the precursor solution to the top of the salt template, it was quickly pushed through the mold with compressed air and then exposed to UV light. Using this method, templated $PDMS_{star}$-PEG hydrogels were prepared with low sol content values (<5 wt%) indicating effective photocuring (Table S1).

### 3.2. $PDMS_{star}$-MA distribution and scaffold morphology

Distribution of $PDMS_{star}$-MA within the templated SIPS $PDMS_{star}$-PEG hydrogels was examined by CLSM imaging with hydrophobic $PDMS_{star}$-MA-rich regions stained by hydrophobic Nile red dye. For the fabrication of non-templated $PDMS_{star}$-PEG hydrogels, an aqueous precursor solution produced exclusively discrete $PDMS_{star}$-MA-rich microparticles within a PEG-DA matrix [22], whereas SIPS fabrication produced a much more uniform distribution [20]. In general, the templated SIPS $PDMS_{star}$-PEG hydrogels exhibited $PDMS_{star}$-MA distribution throughout the pore walls (Fig. 1). This was attributed to the improved solubility of $PDMS_{star}$-MA in DCM versus in water, even at higher precursor solution concentrations. Since solution phase separation increased with $PDMS_{star}$-MA $M_n$, it was expected that the 2k hydrogel series would exhibit a more uniform distribution of $PDMS_{star}$-MA versus the 7k series. Indeed, the 7k series showed the presence of $PDMS_{star}$-MA-rich microdroplets that was not observed for the 2k series.

SEM was used to visually confirm pore interconnectivity of templated SIPS $PDMS_{star}$-PEG hydrogels prepared with the different template salt sizes (Fig. 2). While expected differences in pore sizes were apparent depending on template salt size, the measured average pore size was reduced due to specimen shrinkage associated with vacuum drying (Table 1). However, SEM images did reveal pore interconnectivity, a product of the fused salt template. Pore size for hydrated hydrogels was measured using brightfield microscopy (Fig. 2). As anticipated, hydrated pore sizes were swollen beyond the original salt size of the template (Table 1).

To quantify interconnectivity of hydrated specimens, a water wicking test was adapted from *Bencherif et al.* [34]. Templated SIPS $PDMS_{star}$-PEG hydrogels (20:80 wt/wt % and 2k $PDMS_{star}$-MA) were compared to the analogous non-templated SIPS hydrogels as well as conventionally fabricated hydrogels (i.e. from an aqueous precursor solution) (Fig. 3A) [20,

22]. For the templated hydrogel only, due to its high pore interconnectivity, water was quickly wicked away using a Kimwipe and pore interconnectivity was >50% (Fig. S3). In contrast, conventionally and SIPS fabricated, non-templated $PDMS_{star}$-PEG hydrogels demonstrated interconnectivity below 15%.

### 3.3. Material characterization

To assess the impact of $PDMS_{star}$-MA concentration (0:100, 10:90, 20:80 and 30:70 wt/wt % $PDMS_{star}$-MA:PEG-DA) and $M_n$ (2k or 7k), templated SIPS $PDMS_{star}$-PEG hydrogels were prepared with the intermediate salt size (medium salt, ~270 μm) and subjected to characterization of key properties – hydration, modulus and degradation rate. Because the hydration (i.e. equilibrium swelling) is known to profoundly impact most hydrogels' mechanical and degradation properties [37, 38], this was initially measured (Fig. 3B).

All hydrogels exhibited statistically similar swelling ratios (~13) compared to the analogous templated SIPS PEG-DA control. It is hypothesized that the high pore volume and resulting high water content effectively masked any contribution from pore wall hydrophobicity based on $PDMS_{star}$-MA content, $M_n$ or its distribution therein. As expected, it was noted that the high pore volume of these templated SIPS hydrogels produced a significantly higher swelling ratio versus the analogous non-templated SIPS $PDMS_{star}$-PEG hydrogels (~8) [20].

The bulk compressive modulus of these templated SIPS $PDMS_{star}$-PEG hydrogels was also assessed (Fig. S4). All hydrogels displayed similar moduli (~8 kPa) that were not statistically different versus the analogous PEG-DA control. This may be attributed to their similar high bulk hydration (i.e. swelling), resulting from their macroporosity. However, additional mechanical analyses were conducted that were anticipated to reveal differences among hydrogels based on the $PDMS_{star}$-MA content and $M_n$ that comprised the pore walls. An indicator of the damping or energy absorption ability of a material, tan δ (based on the ratio of loss [G"] and storage [G'] moduli) was also measured (Fig. 3C). In this case, templated SIPS hydrogels based on 2k $PDMS_{star}$-MA produced a reduction in tan δ versus the PEG-DA control whereas those based on 7k $PDMS_{star}$-MA did not. The more homogeneous distribution of 2k $PDMS_{star}$-MA within the PEG-DA matrix of the pore walls (Fig. 1) is believed to give rise to this difference in damping. Thus, when the $PDMS_{star}$-MA is not uniformly distributed (i.e. for 7k), the resulting hydrogels retain more of the native properties of the PEG-DA control. Next, AFM was used to probe the local modulus values for templated SIPS $PDMS_{star}$-PEG hydrogels based on 2k $PDMS_{star}$-MA. Versus bulk analyses, AFM has been used to measure the local modulus of scaffold of the pore walls at a scale commensurate with cellular interaction [3]. Per Fig. 3D, the uniform dispersion of 2k $PDMS_{star}$-MA within the templated SIPS $PDMS_{star}$-PEG hydrogels was determined to decrease the Young's modulus values versus the analogous PEG-DA control. Despite this decrease, however, modulus values (~15 kPa) within the range associated with osteogenesis [31, 39].

The relative differences in degradation rates of templated SIPS $PDMS_{star}$-PEG hydrogels versus the analogous PEG-DA control was assessed by measuring mass loss under accelerated (basic) conditions (Fig. S5). Despite the introduction of hydrophobic $PDMS_{star}$-MA, no distinguishable differences in mass loss were observed, irrespective of $PDMS_{star}$-

MA content, at all time points. This is attributed to their similarities in pore size (Fig. 2) and bulk swelling (Fig. 3B) that dominate any contributions from the hydrophobic comacromer. However, based on the known accelerated degradation of porous materials having larger pore sizes [40, 41] and our previous studies with templated SIPS PEG-DA scaffolds of varying pore sizes [29], increasing and decreasing the pore size of these templated hydrogels is expected to increase and decrease degradation rates, respectively.

### 3.4. Bioactivity

Bioactivity can be examined *in vitro* by exposing hydrogels to conditions that mimic the implant environment (i.e. ionic concentration, pH and temperature) via soaking in simulated body fluid (SBF, 1X) at 37 °C [35]. A series of templated SIPS hydrogels were prepared with 2k $PDMS_{star}$-MA of varying concentrations (0:100, 10:90, 20:80 and 30:70 wt/wt % $PDMS_{star}$-MA:PEG-DA) using the intermediate salt size (medium salt, ~270 μm). All $PDMS_{star}$-PEG hydrogels exhibited mineralization after 4 weeks of incubation while the analogous PEG-DA control showed none (Fig. 4). XRD confirmed that observed mineral present was hydroxyapatite (HAp) with peaks at 31.7, 45.3, and 56.2 indicating reflections from 112, 222 and 004 crystal planes, respectively [20, 42–44]. Thus, the presence of inorganic $PDMS_{star}$-MA introduced bioactivity to the otherwise biologically inert PEG-DA hydrogel.

### 3.5. Cytotoxicity, cell seeding distribution and cellular morphology

All cell-contacting templated SIPS $PDMS_{star}$-PEG scaffolds and the analogous PEG-DA control (prepared with medium salt; ~270 μm) were made with ACRL-PEG-RGDS for controlled cell adhesion and induction. Cytotoxicity was determined by LDH assay after 48 hr culture with hBMSCs (Fig. 5). Normalized to the corresponding templated SIPS PEG-DA control, all $PDMS_{star}$-MA-containing hydrogels (2k and 7k) were determined to be non-cytotoxic. To verify consistent cell seeding distribution, SYBR green DNA staining was used to visualize cells. Further staining with DAPI and rhodamine phalloidin indicated that cells were elongated and spread along the pore walls, as expected with the presence of the cell adhesion ligand RGDS (Fig. 5 **and** S7). Finally, cell morphology and abundance were similar for all $PDMS_{star}$-PEG scaffold compositions compared to the PEG-DA control (Fig. 5 **and** S7). Thus, all compositions were subsequently subjected to 14-day culture for examination of intrinsic osteoinductivity.

### 3.6. Scaffold-induced osteogenesis of hBMSCs

RGD-containing, templated SIPS $PDMS_{star}$-PEG scaffolds (prepared with medium salt; ~270 μm) were evaluated for their potential to control hBMSC fate by evaluating the relative presence of ECM molecules relevant to osteogenesis after a 14-day culture. Protein level multiplex analysis was conducted to determine relative levels of collagen 1, the primary collagen found in bone, and osteonectin (secreted protein acidic and rich in cysteine or SPARC), a calcium-binding glycoprotein found in bone (Fig. 6A **&** B). All templated SIPS $PDMS_{star}$-PEG scaffolds displayed evidence of $PDMS_{star}$-MA-dose dependent osteogenesis. For those based on 7k $PDMS_{star}$-MA, a 30:70 (wt/wt %) was associated with an increase in collagen 1 and SPARC relative to the analogous PEG-DA control. Scaffolds containing 2k

PDMS$_{star}$-MA also displayed significant increases in collagen I and SPARC but at 20:80 (wt/wt %). However, when 2k PDMS$_{star}$-MA content was increased to a 30:70 (wt/wt %), collagen 1 and SPARC production fell below that of the PEG-DA control. Relative DNA levels tested verified that no significant cell death occurred for this particular scaffold (Fig. S7). Thus, we speculate that the more uniform dispersion of 2k PDMS$_{star}$-MA at this high concentration (30:70 wt/wt %) may have impacted scaffold surface hydrophobicity, resulting in protein adhesion inhibiting function of RGD receptors.

Given the enhanced osteogenesis observed with templated SIPS PDMS$_{star}$-PEG scaffolds based on 2k PDMS$_{star}$-MA at 20:80 (wt/wt %), further studies were conducted for the 2k scaffold series. Specifically, levels of osteopontin (OPN), a bone ECM protein involved in biomineralization, and bone morphogenic protein 2 (BMP-2), a potent osteogenic growth factor, were analyzed by immunoassay. Although no statistical differences were observed for BMP-2 expression levels, the 20:80 (wt/wt %) scaffold supported a ~1.5-fold increase in OPN levels relative to the PEG-DA control (Fig. S8). However, when 2k PDMS$_{star}$-MA levels were further increased to 30:70 (wt/wt %), OPN levels were reduced below that of the 10:90 and 20:80 (wt/wt %) formulations as seen previously with collagen I and SPARC (Fig. 6A&B). Von Kossa staining was used as a visual indicator of matrix mineralization and also revealed considerable enhancement in calcium deposition with increasing 2k PDMS$_{star}$-MA content (represented by a brown-black color) (Fig. 6C ). Despite the reductions in collagen 1, SPARC, and BMP-2 noted for the 30:70 (wt/wt %) scaffold, this formulation appeared to support increased mineralization relative to remaining formulations, denoting a possible disconnect between bioactivity and osteoinductivity of the scaffold based on distribution of the PDMS$_{star}$-MA.

## 4. Conclusions

Herein, we describe the preparation of templated SIPS PDMS$_{star}$-PEG hydrogels and their utility as instructive scaffolds (absent of exogenous growth factors) for bone regeneration. These hydrogels utilized an inorganic hydrophobic comacromer, PDMS$_{star}$-MA, to introduce bioactivity and osteoinductivity. Fabrication with a fused salt template, in conjunction with SIPS employing a DCM precursor solution (followed by drying and hydration), created interconnected macropores of tunable sizes to permit post-fabrication cell seeding and for osteoconductivity. Hydrogels were produced with two $M_n$'s of PDMS$_{star}$-MA (2k and 7k) and varying wt/wt % ratios (0:100, 10:90, 20:80, and 30:70) of PDMS$_{star}$-MA to PEG-DA ($M_n$ = 3.4k). CLSM images revealed the improved distribution of the 2k PDMS$_{star}$-MA within the PEG matrix, attributed to its superior solubility in the DCM precursor solution. Pore size tunability and interconnectivity for osteoconductivity were confirmed by SEM imaging and a water wicking test. Templated SIPS PDMS$_{star}$-PEG hydrogels all had similarly high bulk hydration, resulting in similar bulk Young's moduli. However, for the 2k-containing scaffolds, a lower modulus was seen at a local level (via AFM probe measurement), but they remained in the range associated with osteogenesis in hydrogels. While absent for the PEG-DA control, bioactivity was confirmed for templated SIPS PDMS$_{star}$-PEG hydrogels (2k series) with HAp formation observed (via SEM and XRD) following soaking in SBF. Under accelerated conditions, owing to their similarity in pore size and bulk swelling, these hydrogels exhibited temporal mass loss similar to that of the

PEG-DA control. Finally, all RGD-containing templated SIPS $PDMS_{star}$-PEG scaffolds were confirmed non-cytotoxic and showed PDMS dose-dependent increases in key indicators of osteogenesis. However, this was dependent on comacromer $M_n$, wherein the better dispersed comacromer (lower $M_n$) showed statistical differences at lower concentrations. Von Kossa staining was used to reveal dose-dependent increases in calcium deposition by hBMSCs seeded on 2k-containing scaffolds. Overall, these templated SIPS $PDMS_{star}$-PEG hydrogels displayed the potential to serve as instructive scaffolds for bone regeneration without the inclusion of added growth factors. The achievement of the observed bioactivity and osteoinductivity without the inclusion of glass or glass-ceramic fillers but rather a polymeric component (i.e. $PDMS_{star}$-MA) is notable.

## Supplementary Material

Refer to Web version on PubMed Central for supplementary material.

## Acknowledgements

M.T.F. gratefully acknowledges funding from the Texas A&M University Office of Graduate and Professional Studies. The use of the Materials Characterization Facility and the Microscopy and Imaging Center at Texas A&M University is acknowledged. The Olympus FV1000 confocal microscope acquisition was supported by the Office of the Vice President for Research at Texas A&M University. The graphical abstract utilized elements from Servier Medical Art, provided by Servier, licensed under a Creative Commons Attribution 3.0 unported license (http://smart.servier.com).

Funding

This work was supported by the American Kennel Club (#02078), Texas A&M Engineering Experiment Station (TEES) and NIH/NIDCR (1R01DE025886-01A1).

## References

[1]. Dutta RC, Dutta AK, Cell-interactive 3D-scaffold; advances and applications, Biotechnology Advances 27 (2009) 334–339. [PubMed: 19232387]

[2]. Lutolf MP, Hubbell JA, Synthetic biomaterials as instructive extracellular microenvironments for morphogenesis in tissue engineering, Nature Biotechnology 23 (2005) 4315–4323.

[3]. Brandi F, Sommer F, Goepferich A, Rational design of hydrogels for tissue engineering: Impact of physical factors on cell behavior, Biomaterials 28 (2007) 134–6. [PubMed: 17011028]

[4]. Weisgerber DW, Caliari SR, Harley BA, Mineralized collagen scaffolds induce hMSC osteogenesis and matrix remodeling, Biomaterials science 3(3) (2015) 533–42. [PubMed: 25937924]

[5]. Vo TN, Kasper FK, Mikos AG, Strategies for Controlled Delivery of Growth Factors and Cells for Bone Regeneration, Advanced Drug Delivery Reviews 64(12) (2012) 1292–1309. [PubMed: 22342771]

[6]. Lyons FG, Gleeson JP, Partap S, Coghlan K, O'Brien FJ, Novel microhydroxyapatite particles in a collagen scaffold: a bioactive bone void filler?, Clinical Orthopaedics and Related Research 472(4) (2014) 1318–28. [PubMed: 24385037]

[7]. Amini AR, Laurencin CT, Nukavarapu SP, Bone Tissue Engineering: Recent Advances and Challenges, Critical Reviews in Biomedical Engineering 40(5) (2012) 363–408. [PubMed: 23339648]

[8]. Stevens MM, Biomaterials for bone tissue engineering, Materials Today 11(5) (2008) 18–25.

[9]. Albrektsson T, Johansson C, Osteoinduction, osteoconduction and osseointegration, European Spine Journal 10(2) (2001) S96–S101. [PubMed: 11716023]

[10]. Roseti L, Parisi V, Petretta M, Cavallo C, Desando G, Bartolotti I, Grigolo B, Scaffolds for Bone Tissue Engineering: State of the art and new perspectives, Materials Science and Engineering: C 78 (2017) 1246–1262. [PubMed: 28575964]

[11]. Hutmacher DW, Scaffolds in tissue engineering bone and cartilage, Biomaterials 21(24) (2000) 2529–2543. [PubMed: 11071603]

[12]. Bružauskaitė I, Bironaitė D, Bagdonas E, Bernotienė E, Scaffolds and cells for tissue regeneration: different scaffold pore sizes—different cell effects, Cytotechnology 68(3) (2016) 355–369. [PubMed: 26091616]

[13]. Dinarvand P, Seyedjafari E, Shafiee A, Babaei Jandaghi A, Doostmohammadi A, Fathi MH, Farhadian S, Soleimani M, New Approach to Bone Tissue Engineering: Simultaneous Application of Hydroxyapatite and Bioactive Glass Coated on a Poly(l-lactic acid) Scaffold, ACS Applied Materials & Interfaces 3(11) (2011) 4518–4524. [PubMed: 21999213]

[14]. Rezwan K, Chen QZ, Blaker JJ, Boccaccini AR, Biodegradable and bioactive porous polymer/inorganic composite scaffolds for bone tissue engineering, Biomaterials 27 (2006) 3413–3431. [PubMed: 16504284]

[15]. Wang W, Yeung KWK, Bone grafts and biomaterials substitutes for bone defect repair: A review, Bioactive Materials 2(4) (2017) 224–247. [PubMed: 29744432]

[16]. Ayala R, Zhang C, Yang D, Hwang Y, Aung A, Shroff SS, Arce FT, Lai R, Arya G, Varghese S, Engineering the cell-material interface for controlling stem cell adhesion, migration, and differentiation, Biomaterials 32 (2011) 3700–3711. [PubMed: 21396708]

[17]. Fu Q, Saiz E, Rahaman MN, Tomsia AP, Bioactive glass scaffolds for bone tissue engineering: state of the art and future perspectives, Materials Science and Engineering: C 31(7) (2011) 1245–1256. [PubMed: 21912447]

[18]. Kim E-J, Bu S-Y, Sung M-K, Choi M-K, Effects of Silicon on Osteoblast Activity and Bone Mineralization of MC3T3-E1 Cells, Biological Trace Element Research 152(1) (2013) 105–112. [PubMed: 23306944]

[19]. Beck GR, Ha S-W, Camalier CE, Yamaguchi M, Li Y, Lee J-K, Weitzmann MN, Bioactive silica based nanoparticles stimulate bone forming osteoblasts, suppress bone esorbing osteoclasts, and enhance bone mineral density in vivo, Nanomedicine 8(6) (2012) 793–803. [PubMed: 22100753]

[20]. Bailey BM, Fei R, Munoz-Pinto D, Hahn MS, Grunlan MA, $PDMS_{star}$-PEG hydrogels prepared via solvent-induced phase separation (SIPS) and their potential utility as tissue engineering scaffolds, Acta Biomaterialia 8 (2012) 4324–4333. [PubMed: 22842033]

[21]. Munoz-Pinto DJ, Jimenez-Vergara AC, Hou Y, Hayenga HN, Rivas A, Grunlan M, Hahn MS, Osteogenic potential of poly(ethylene glycol)-poly(dimethylsiloxane) hybrid hydrogels, Tissue Engineering Part A 18(15-16) (2012)1710–9. [PubMed: 22519299]

[22]. Hou Y, Schoener CA, Regan KR, Munoz-Pinto D, Hahn MS, Grunlan MA, Photo-Cross-Linked PDMSstar-PEG Hydrogels: Synthesis, Characterization, and Potential Application for Tissue Engineering Scaffolds, Biomacromolecules 11(3) (2010) 648–656. [PubMed: 20146518]

[23]. Zhu J, Bioactive modification of poly(ethylene glycol) hydrogels for tissue engineering, Biomaterials 31(17) (2010) 4639–4656. [PubMed: 20303169]

[24]. Drury JL, Mooney DG, Hydrogels for tissue engineering: Scaffold design variables and applications, Biomaterials 24 (2003) 4337–4351. [PubMed: 12922147]

[25]. Mann BK, Gobin AS, Tsai AT, Schmedlen RH, West JL, Smooth muscle cell growth in photopolymerized hydrogels with cell adhesive and proteolytically degradable domains: Synthetic ECM analogs for tissue engineering, Biomaterials 22 (2001) 3045–3051. [PubMed: 11575479]

[26]. Bailey BM, Hui V, Fei R, Grunlan MA, Tuning PEG-DA hydrogel properties via solvent-induced phase separation (SIPS), Journal of Materials Chemistry 21 (2011) 18776–18782. [PubMed: 22956857]

[27]. Murphy WL, Dennis RG, Kileny JL, Mooney DJ, Salt fusion: An approach to improve pore interconnectivity within tissue engineering scaffolds, Tissue Engineering 8(1) (2002) 43–52. [PubMed: 11886653]

[28]. Zhang D, Burkes WL, Schoener CA, Grunlan MA, Porous inorganic–organic shape memory polymers, Polymer 53(14) (2012) 2935–2941. [PubMed: 22956854]

[29]. Gacasan EG, Sehnert RM, Ehrhardt DA, Grunlan MA, Templated, Macroporous PEG-DA Hydrogels and Their Potential Utility as Tissue Engineering Scaffolds, Macromolecular Materials and Engineering (2017) 1600512.

[30]. Discher DE, Janmey P, Wang Y-I, Tissue cells feel and respond to the stiffness of their substrate, Science 310 (2005) 1139–1143. [PubMed: 16293750]

[31]. Engler AJ, Sen S, Sweeney HL, Discher DE, Matrix elasticity directs stem cell lineage specification, Cell 126 (2006) 677–689. [PubMed: 16923388]

[32]. Escobar-Ivirico JL, Salmeron-Sanchez M, Gomez-Ribelles JL, Monleon-Pradas M, Soria JM, Gomes ME, Reis RL, Mano JF, Proliferation and differentiation of goat bone marrow stromal cells in 3D scaffolds with tunable hydrophilicity, Journal of Biomedical Materials Research Part B: Applied Biomaterials 91B (2009) 277–286.

[33]. Fisher JP, Lalani Z, Bossano CM, Brey EM, Demian N, Johnston CM, Dean D, Jansen JA, Wong ME, Mikos AG, Effect of biomaterial properties on bone healing in a rabbit tooth extration socket model, Journal of Biomedical Materials Research Part A 68 (2004) 428–438. [PubMed: 14762922]

[34]. Bencherif SA, Sands RW, Bhatta D, Arany P, Verbeke CS, Edwards DA, Mooney DJ, Injectable preformed scaffolds with shape-memory properties, Proceedings of the National Academy of Sciences of the United States of America 109(48) (2012) 19590–19595. [PubMed: 23150549]

[35]. Kokubo T, Takadama H, How useful is SBF in predicting in vivo bone bioactivity?, Biomaterials 27 (2006) 2907–2915. [PubMed: 16448693]

[36]. Burdick JA, Anseth KS, Photoencapsulation of osteoblasts in injectable RGD-modified PEG hydrogels for bone tissue engineering, Biomaterials 23 (2002) 4315–4323. [PubMed: 12219821]

[37]. Anseth KS, Bowman CN, Brannon-Peppas L, Mechanical properties of hydrogels and their experimental determination, Biomaterials 17(17) (1996) 1647–1657. [PubMed: 8866026]

[38]. Griffith LG, Polymeric biomaterials, Acta Materialia 48(1) (2000) 263–277.

[39]. Huebsch N, Arany PR, Mao AS, Shvartsman D, Ali OA, Bencherif SA, Rivera-Feliciano J, Mooney DJ, Harnessing traction-mediated manipulation of the cell/matrix interface to control stem-cell fate, Nature Materials 9 (2010) 518. [PubMed: 20418863]

[40]. Wu L, Ding J, Effects of porosity and pore size on *in vitro* degradation of three-dimensional porous poly(D,L-lactide-*co*-glycolide) scaffolds for tissue engineering, Journal of Biomedical Materials Research Part A 75A (2005) 767–777.

[41]. Karageorgiou V, Kaplan D, Porosity of 3D biomaterial scaffolds and osteogenesis, Biomaterials 26 (2005) 5474–5491. [PubMed: 15860204]

[42]. Sobhana SSL, Sundaraseelan J, Sekar S, Sastry TP, Mandal AB, Gelatin–Chitosan composite capped gold nanoparticles: a matrix for the growth of hydroxyapatite, Journal of Nanoparticle Research 11(2)(2008)333–340.

[43]. Dinh TMT, Nguyen TT, Pham TN, Nguyen TP, Nguyen TTT, Hoang T, Grossin D, Bertrand G, Drouet C, Electrodeposition of HAp coatings on Ti6Al4V alloy and its electrochemical behavior in simulated body fluid solution, Advances in Natural Sciences: Nanoscience and Nanotechnology 7(2) (2016)025008.

[44]. Liu S, Liu G, Wei W, Xiangli F, Jin W, Ceramic Supported PDMS and PEGDA Composite Membranes for CO2 Separation, Chinese Journal of Chemical Engineering 21(4) (2013) 348–356.

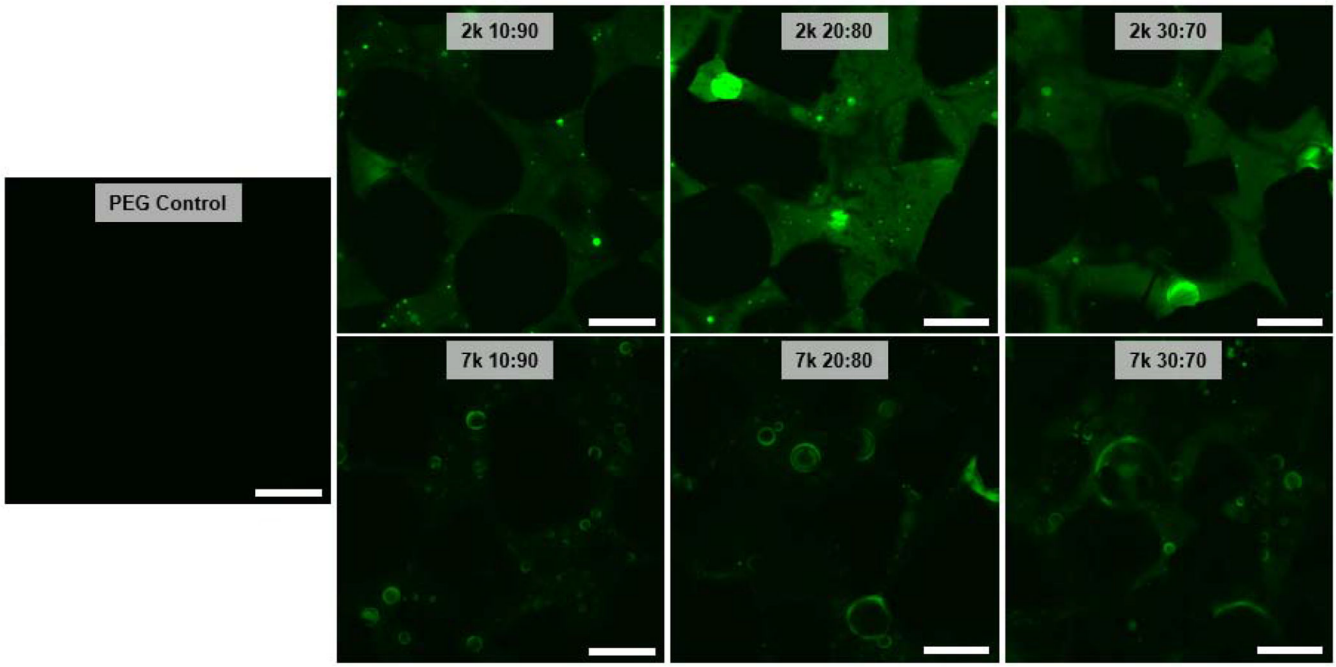


**Figure 1.**

CLSM images of templated SIPS $PDMS_{star}$-PEG hydrogels prepared with increasing amounts of 2k and 7k $PDMS_{star}$-MA and a templated PEG control. All hydrogels prepared with medium salt (~270 μm). Green is assigned to $PDMS_{star}$-MA-rich regions, stained by hydrophobic dye (Nile red). Photos are adjusted +20% brightness and −20% contrast for clarity. Scale bars = 250 μm.

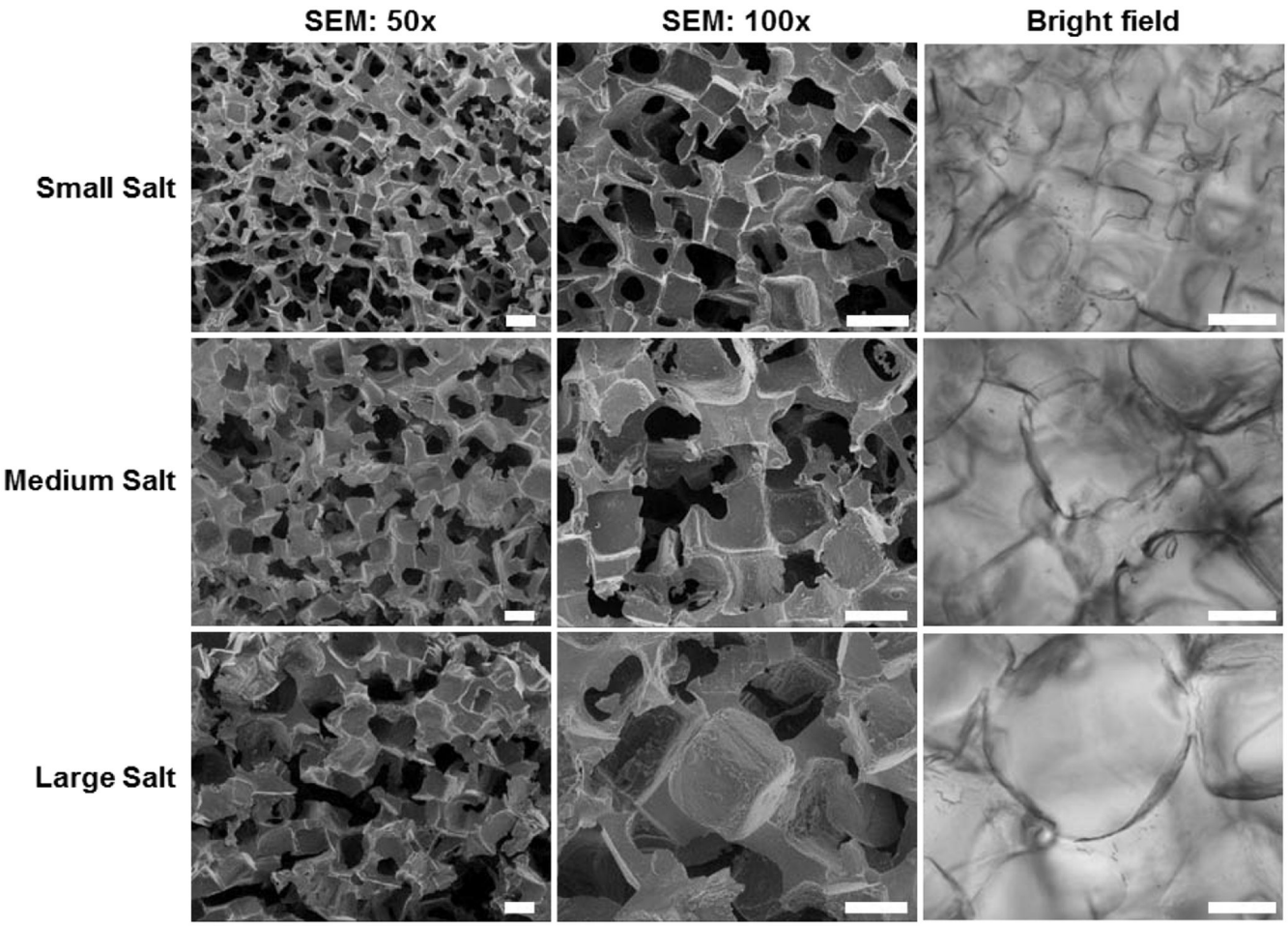


**Figure 2.**

SEM images of templated SIPS $PDMS_{star}$-PEG hydrogels fabricated with each salt size [20:80 wt/wt % and 2k $PDMS_{star}$-MA] (**left and middle column**). Representative bright field images were taken during confocal imaging (**right column**). Scale bars = 200 μm.

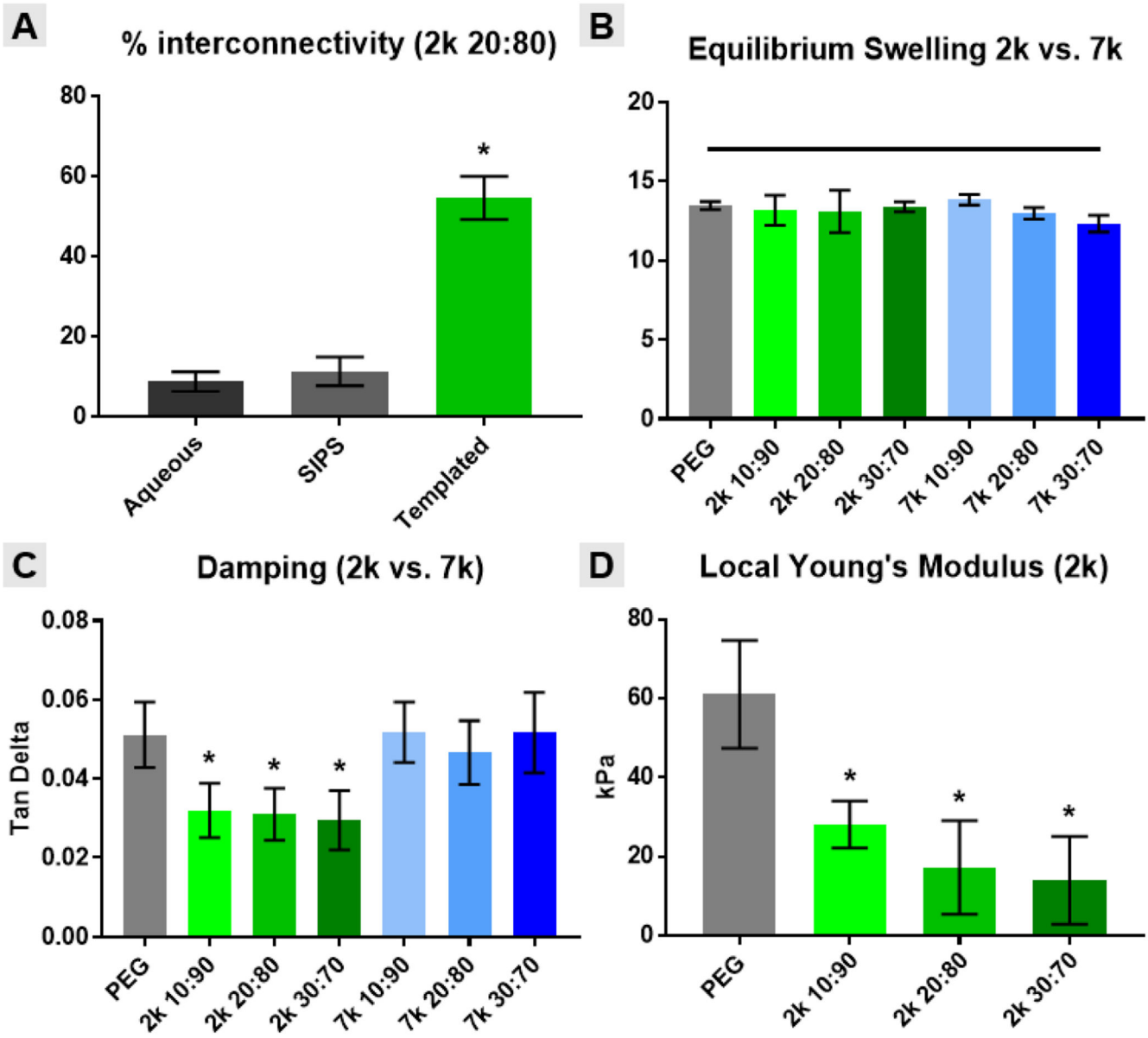


**Figure 3.**

Templated SIPS $PDMS_{star}$-PEG hydrogels and analogous PEG-DA control material properties: **(A)** % interconnectivity, **(B)** equilibrium swelling, **(C)** damping and **(D)** local Young's modulus. All hydrogel scaffolds were fabricated with medium salt (~270 μm). Statistical difference versus the analogous templated SIPS PEG-DA control is represented as * = $p < 0.05$.

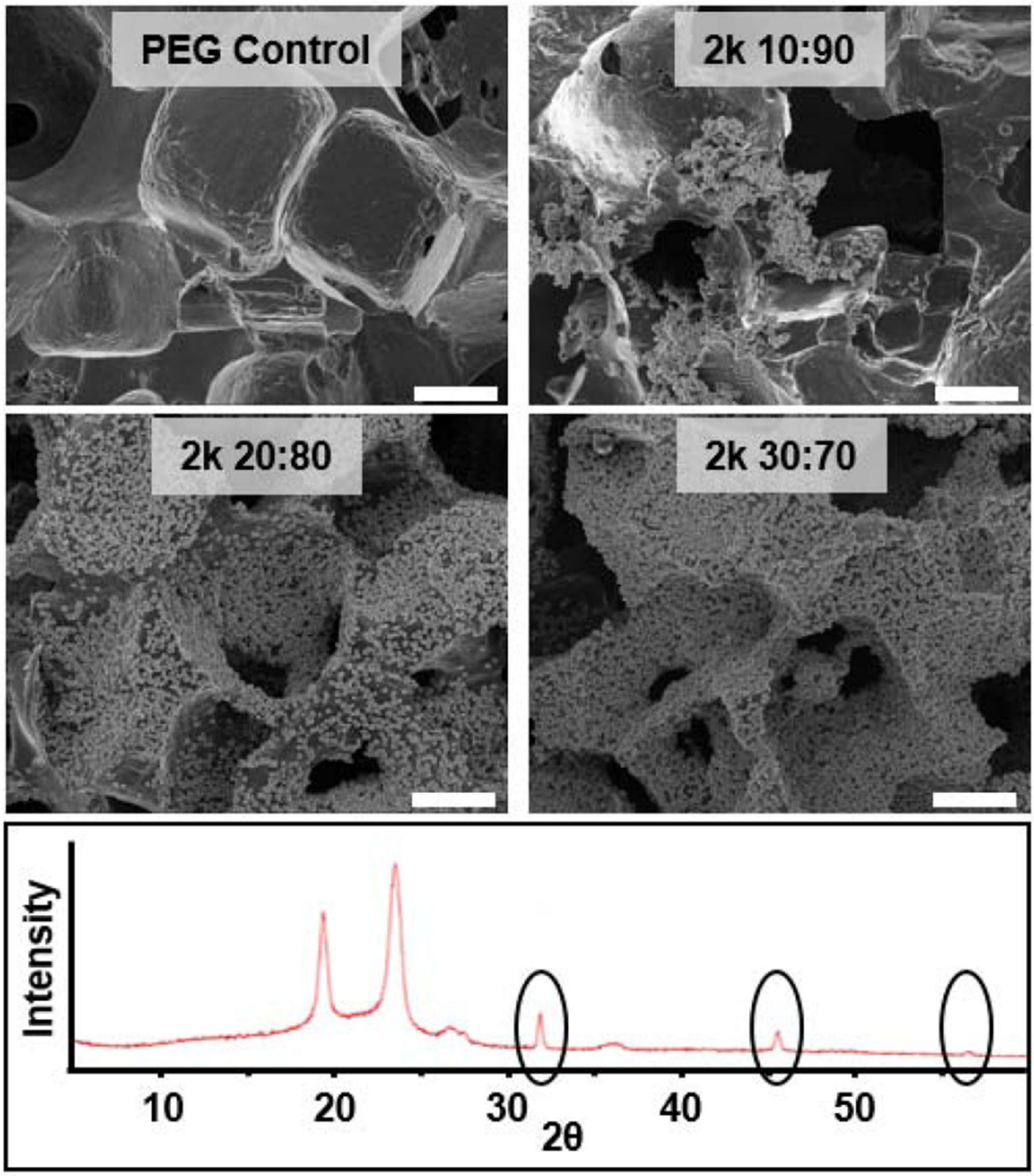


**Figure 4.**

Templated SIPS $PDMS_{star}$-PEG hydrogel and analogous PEG-DA control following exposure to simulated body fluid (SBF, 1X, 537 °C, 4 weeks). Hydrogels were fabricated with medium salt (~270 μm) and 2k $PDMS_{star}$-MA. SEM images (**top**) displayed HAp growth on all $PDMS_{star}$-MA-containing hydrogels. XRD analysis of "20:80 wt/wt %" composition (**bottom**) confirmed HAp identity by characteristic peaks at 31.7, 45.5 and 56.5. Scale bar = 100 μm.

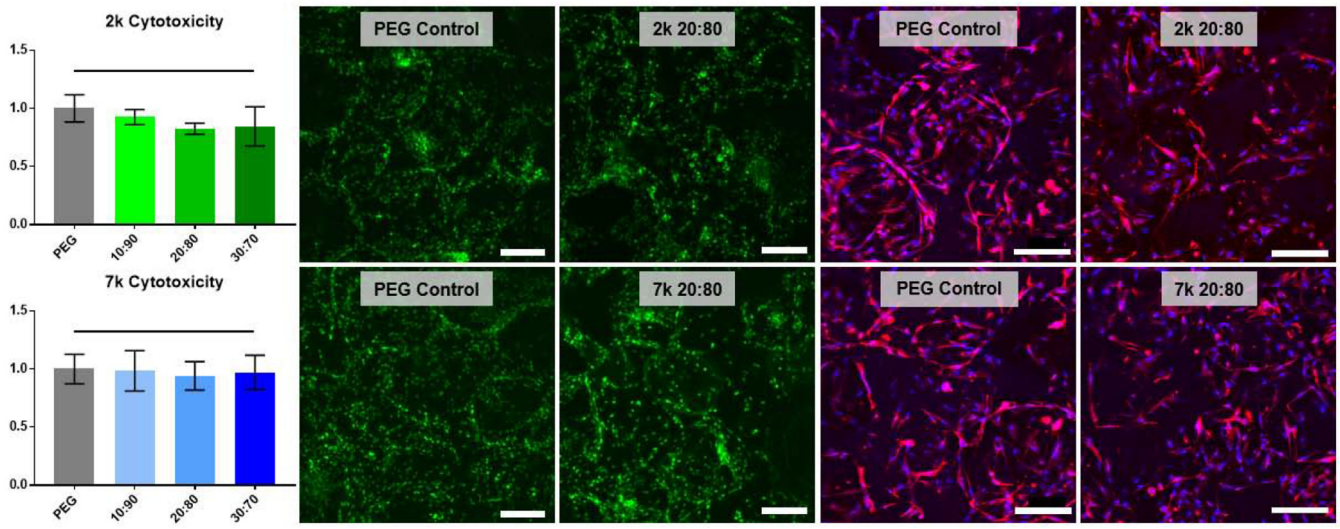


**Figure 5.**

Scaffold non-cytotoxicity after 48 hr culture with hBMSCs, as determined by LDH assay (**left**), SYBR green stain (**middle**) and rhodamine phalloidin (red) and DAPI (blue) stacked confocal images (**right**). Statistically significant difference compared to the control is represented as * = $p$ <0.05. The complete set of images can be found in Fig. S6. All templated SIPS $PDMS_{star}$-PEG and analogous PEG-DA control scaffolds were prepared with medium salt (~270 μm). Scale bars = 200 μm.

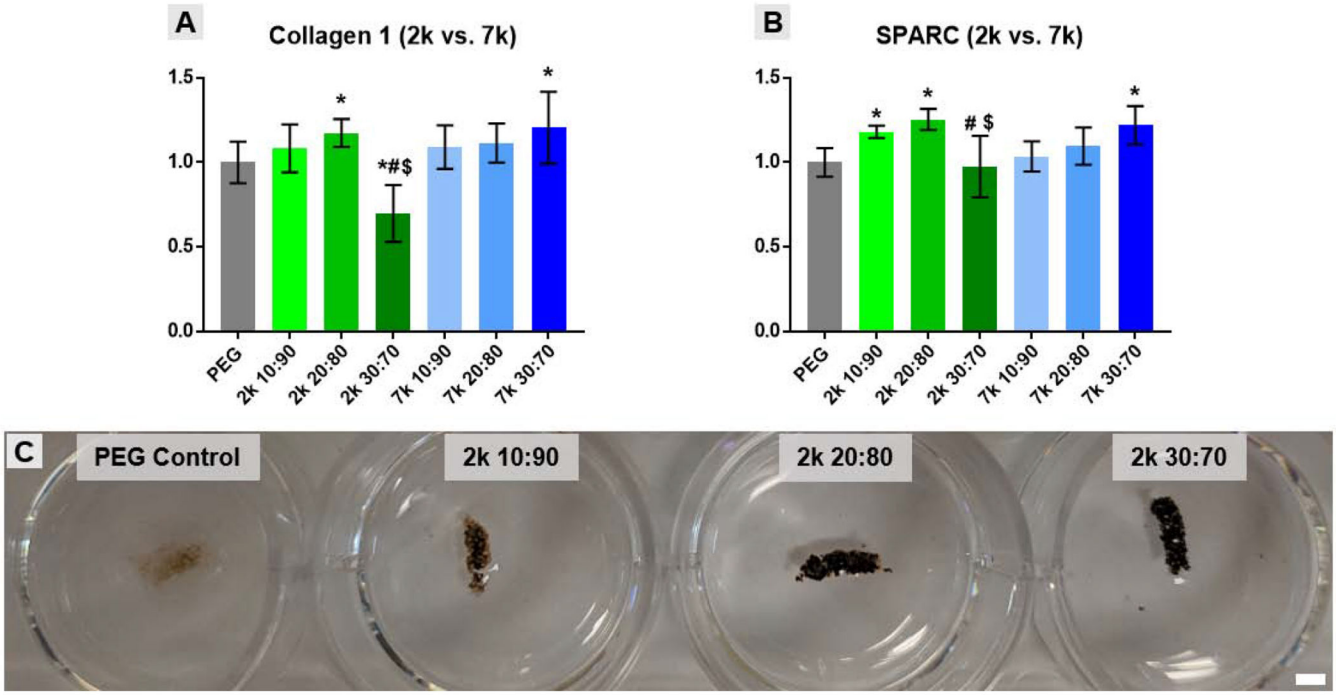


**Figure 6.**

Protein-level multiplex immunoassay results for (**A**) Collagen 1 and (**B**) SPARC presence after 14-day culture on templated SIPS $PDMS_{star}$-PEG and analogous PEG-DA control scaffolds were prepared with medium salt (~270 μm). (**C**) Von Kossa staining (brown-black color) for mineralization after 14 day culture with hBMSCs on scaffolds prepared with 2k $PDMS_{star}$-MA. Due to the intensity of staining, only macro-images could be taken due to over-saturation during imaging. Statistically significant difference compared to the control is represented as * = $p$ <0.05, to the corresponding 10:90 (wt/wt %) as # = $p$ < 0.05, and to the corresponding 20:80 as $ = $p$ < 0.05. Scale bar = 2 mm.

**Table 1.**

Pore size measurements of templated SIPS $PDMS_{star}$-PEG hydrogels fabricated with each template salt size [20:80 wt/wt % and 2k $PDMS_{star}$-MA] determined by ImageJ software using SEM images (acquired at 100x magnification) for “dry” measurements [i.e. after vacuum drying] and bright field microscopy images for “hydrated’ measurements [i.e. in the hydrated state].

| | SMALL SALT | MEDIUM SALT | LARGE SALT |
|---|---|---|---|
| **SALT SIZE:** | 181 ± 29 μm | 268 ± 35 μm | 459 ± 69 μm |
| **DRY:** | 124 ± 17 μm | 199 ± 13 μm | 282 ± 60 μm |
| **HYDRATED:** | 268 ± 19 μm | 367 ± 16 μm | 428 ± 60 μm |